Thermophysical Algebraic Invariants from Infrared Imagery for Object Recognition*

J. Michel[†], michel@Virginia.EDU
N. Nandhakumar[†], nandhu@Virginia.EDU
V. Velten[‡] vvelten@mbvlab.wpafb.af.mil

[†] Dept of Electrical Engineering, Univ. of Virginia, Charlottesville, VA 22903

[‡] USAF Wright Laboratory - Advanced Avionics, WPAFB, OH 45433-7001

Abstract

An important issue in developing a model-based vision system is the specification of features that are - (a) invariant to viewing and scene conditions, and also - (b) specific, i.e., the feature must have different values for different classes of objects. We formulate a new approach for establishing invariant features. Our approach is unique in the field since it considers not just surface reflection and surface geometry in the specification of invariant features, but it also takes into account internal object composition and state which affect images sensed in the non-visible spectrum. A new type of invariance called Thermophysical Invariance is defined. Features are defined such that they are functions of only the thermophysical properties of the imaged objects. The approach is based on a physics-based model that is derived from the principle of the conservation of energy applied at the surface of the imaged object.

*This research was supported by the AFOSR contract F49620-93-C-0063, the AFOSR grant LRIR-93WL001, an AFOSR Laboratory Graduate Fellowship, ARPA contract F33615-94-C-1529 and the National Science Foundation Contract IRI-91109584.

1 Introduction

Non-visible modalities of sensing have been shown to greatly increase the amount of information that can be used for object recognition. A very popular and increasingly affordable sensor modality is thermal imaging - where non-visible radiation is sensed in the long-wave infrared (LWIR) spectrum of $8\mu m$ to $14\mu m$. The current generation of LWIR sensors produce images of contrast and resolution that compare favorably with broadcast television quality visible light imagery. However, the images are no longer functions of only surface reflectance. As the wavelength of the sensor transducer passband increases, emissive effects begin to emerge as the dominant mode of electromagnetic energy exitance from object surfaces. The (primarily) emitted radiosity of LWIR energy has a strong dependence on internal composition, properties, and state of the object such as specific heat, density, volume, heat generation rate of internal sources, etc. This dependence may be exploited by specifying image-derived invariants that vary only if these parameters of the physical properties vary.

In this paper we describe the use of the principle of conservation of energy at the surface of the imaged object to specify a functional relationship between the object's thermophysical properties (e.g., thermal conductivity, thermal capacitance, emissivity, etc.), scene parameters (e.g., wind temperature, wind speed, solar insolation), and the sensed LWIR image gray level. We use this functional form to derive invariant features that remain constant despite changes in scene parameters/driving conditions. In this formulation the internal thermophysical properties play a role that is analogous to the role of parameters of the conics, lines and/or points that are used for specifying geometric invariants (GI's) when analyzing visible wavelength imagery [1]. Thus, in addition to the currently available techniques of formulating features that depend only on external shape [2] - [10], and surface reflectance properties [11] - [16], the phenomenology of LWIR image generation can be used to establish new features that "uncover" the composition

and thermal state of the object, and which do not depend on surface reflectance characteristics.

An intuitive approach to thermo-physical interpretation of LWIR imagery is given in [17]. This approach rests upon the following observation, termed the "Thermal History Consistency Constraint" and analogous to Lowe's well known Viewpoint Consistency Constraint [18]: "The temperature of all target features for a passive target must be consistent with the heat flux transfer resulting from exposure to the same thermal history." In [17] this constraint is exploited by analyzing objects to locate components that are similar in terms of thermo-physical properties and then examining a temporal sequence of calibrated LWIR data to experimentally assess the degree to which such thermo-physically similar components exhibit similar temperature state temporal behavior. Such analysis was shown to lead to formulation of simple intensity ratio features exhibiting a strong degree of temporal stability that could be exploited provided: (1) thermally homogeneous regions in the LWIR image corresponding to the thermo-physically similar object components could be reliably segmented, and (2) a target-specific geometric reference frame is available in order to correctly associate extracted regions with candidate object components.

To avoid the difficulties inherent in assumptions (1) and (2) above an alternative technique applicable to overall object signatures was suggested in [17]. An analysis of typical LWIR 'lumped parameter' object temperature modeling approaches suggests that over small time scales object temperature can be crudely modeled by a small dimensional linear system with algebraically separable spatial and temporal components. Ratios of spatial integrals of temperature with a simple set of orthonormal 2D polynomials (obtained from applying Gramm-Schmidt to $1, x, y, xy, x^2y, xy^2, x^3$ and y^3) were tried. Some of the resulting functions were nearly constant with time when measured against 24 hours of LWIR imagery of a complex object (a tank) but no experimentation was done with multiple objects to examine between and within-class separation, so little can be drawn in the way of a substantive conclusion with respect to utility

as an object identification technique.

A physics-based approach that attempts to establish invariant features which depend only on thermophysical object properties was reported in [19], [20]. A thermophysical model was formulated to allow integrated analysis of thermal and visual imagery of outdoor scenes. This method used estimations of the energy flux into and out of the surface of the object. The surface orientation and absorptivity were obtained from the visual image using a simplified shape-from-shading method. The surface temperature was estimated from the thermal image based on an appropriate model of radiation energy exchange between the surface and the infrared camera. A normalized feature, R, was defined to be the ratio of energy fluxes estimated at each pixel. The value of R was lowest for vehicles, highest for vegetation and in between for buildings and pavements. This approach is powerful in that it makes available features that are completely defined by internal object properties. The computed value of R may be compared with accurate *ground truth* values computed from known physical properties of test objects – one of the major advantages of using physics-based/phenomenological models as compared to statistical models. Classification of objects using this property value is discussed in [21], [22].

There are several factors that limit the performance of the above thermophysical approach. The thermal and visual image pairs may not be perfectly registered. Also, segmentation errors typically cause a large portion of an object to be included with small portions of a different object in one region. This results in meaningless values of the surface energy estimates at/near the region boundaries. These errors give rise to a significant number of inaccurate estimates of the surface energy exchange components. The histogram of values of the ratio of energy fluxes tends to be heavy-tailed and skewed. A statistically robust scheme has been proposed to minimize this drawback [22]. However, the computational complexity for such a technique is very high, and the following drawbacks below were not adequately overcome: (1) The value of R was found to be only weakly invariant - while separation between classes was preserved, the

range of values of this feature for each class was observed to vary with time of day and season of year, (2) The feature was able to separate very broad categories of objects, such as automobiles, buildings, and vegetation - but lacked the specificity to differentiate between different models of vehicles. Although the thermophysical feature, R, is limited in its application for recognition, the energy exchange model on which it is based forms the groundwork for the derivation of more powerful thermophysical invariant features. That approach is extended in this paper by applying the concepts of algebraic invariance to the energy exchange model resulting in new thermophysical invariant features for object recognition.

The derivation of thermophysical invariants (TI's) from non-visible wavelength imagery, the evaluation of the performance of these invariants, and their use in object recognition systems poses several advantages. The main advantage of this approach is the potential availability of a number of new (functionally independent) invariants that depend on internal compositional properties of the imaged objects. Note that it is possible to evaluate the behavior of thermophysical invariants using ground truth data consisting of images of objects of known composition and internal state. This additional information can be used to augment/complement the behavior of GI's. One way in which GI's can be integrated with TI's for object recognition is as follows: (1) Parametric curves and/or lines are extracted from an LWIR image. (2) The curves are used to compute GI's which are in turn used to hypothesize object identity and pose, and (3) TI's are computed for this hypothesis and compared to a stored model library for verification. Some details of this approach are presented later. Although the TI's are used solely for the verification of hypothesis generated by other means, this task is of primary importance in a number applications such as site change detection, monitoring, and surveillance.

The ideas presented in this paper are continuations/extensions of previous and ongoing research in thermophysical model-based interpretation of LWIR imagery. A brief description of this thermophysical approach is presented in section 2. The formulation of a new method to

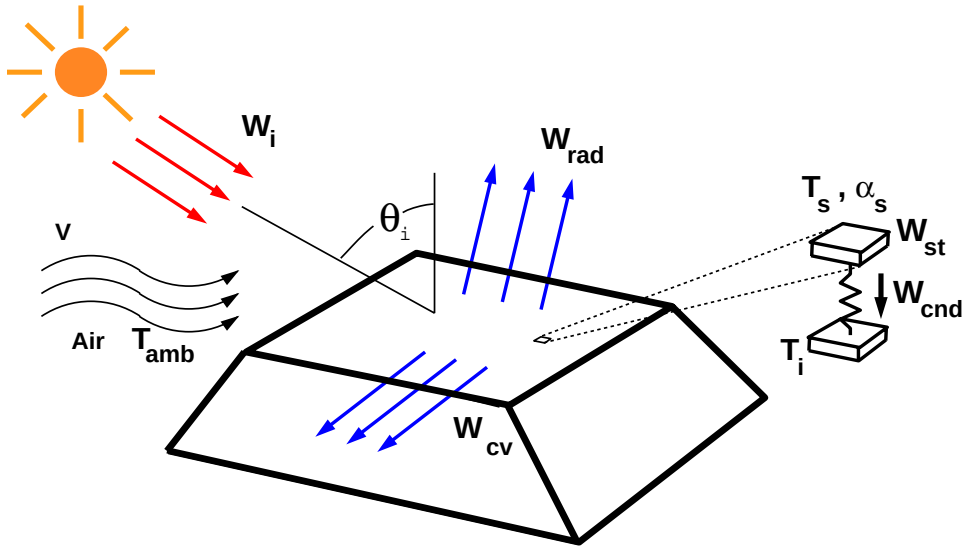

Figure 1: Energy exchange at the surface of the imaged object. Incident energy is primarily in the visible spectrum. Surfaces loses energy by convection to air, and via radiation to the atmosphere. An elemental volume at the surface is shown. Some of the absorbed energy raises the energy stored in the elemental volume, while another portion is conducted into the interior of the object.

derive thermophysical invariants is described in section 3. Section 4 describes a context based approach that proposes the thermophysical feature in a hierarchical framework. Experimental results of applying this new approach to real imagery are presented in section 5, which is followed by a discussion of the behavior of the new method, issues to be considered in using this method for object recognition, and issues that remain to be explored.

2 A Thermophysical Approach to IR Image Analysis

Consider an infinitesimal volume at the surface of the imaged object (figure 1). Energy absorbed by the surface equals the energy lost to the environment.

$$W_{abs} = W_{lost} \tag{1}$$

Energy absorbed by the surface (per unit surface area) is given by

$$W_{abs} \;=\; W_I \; cos\theta_I \; \alpha_s \;, \tag{2}$$

where, W_I is the incident solar irradiation on a horizontal surface per unit area and is given by available empirical models (based on time, date and latitude of the scene) or by measurement with a pyranometer, θ_i is the angle between the direction of irradiation and the surface normal, and α_s is the surface absorptivity which is related to the visual reflectance ρ_s by $\alpha_s = 1 - \rho_s$. Note that it is reasonable to use the visual reflectance to estimate the energy absorbed by the surface since approximately 90% of the energy in solar irradiation lies in the visible wavelengths [23].

The energy lost by the surface to the environment was given by

$$W_{lost} \;=\; W_{cnd} \;+\; W_{st} \;+\; W_{cv} \;+\; W_{rad}, \tag{3}$$

where, W_{cv} denotes the energy (per unit surface area) convected from the surface to the air which has temperature T_{amb} and velocity V, W_{rad} is the energy (per unit surface area) lost by the surface to the environment via radiation and W_{cnd} denotes the energy (per unit surface area) conducted from the surface into the interior of the object. The radiation energy loss is computed from:

$$W_{rad} \;=\; \epsilon\, \sigma\, (T_s^4 - T_{amb}^4), \tag{4}$$

where, σ denotes the Stefan-Boltzman constant, T_s is the surface temperature of the imaged object, and T_{amb} is the ambient temperature. Assume ϵ for the atmosphere is equal to ϵ for the imaged object. This assumption is reasonable if the objects are not uncoated metals [24]. This assumption may not hold if the imaged surface is exposed or unoxidized metal which is usually rare.

The convected energy transfer is given by

$$W_{cv} \;=\; h(T_s \;-\; T_{amb}) \tag{5}$$

where, h is the average convected heat transfer coefficient for the imaged surface, which depends on the wind speed, thermophysical properties of the air, and surface geometry [23].

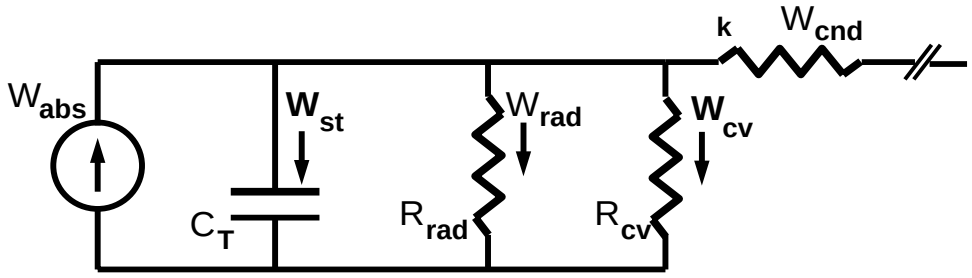

Figure 2: The equivalent thermal circuit for the extended model that separates the stored energy component and the conduction component to the interior of the object.

The equivalent thermal circuit for the surface is shown in figure 2. Lateral conduction from the elemental volume at the surface is assumed negligible since the temperature of the material adjacent to the surface volume under consideration may be assumed to be similar. In general, the internal temperature of the material will be different from that at the surface. The energy flow due to this gradient is expressed as the conducted energy, $W_{cnd} = -k\ dT/dx$, where k is the thermal conductivity of the material, and x is distance below the surface. Since we are considering an elemental volume at the surface this can be written in finite difference form: $W_{cnd} = -k\frac{(T_s - T_{int})}{\Delta x}$, for infinitesimal Δx. W_{cnd} is also expressed in units of energy flowing across unit area.

Within the elemental volume, the temperature is assumed uniform, and the increase in the stored energy given by $W_{st} = C_T \frac{dT_s}{dt}$, where C_T is the thermal capacitance for the material of the elemental surface volume. This is given by $C_T = DVc$, where D is the density of the surface material, V is the elemental volume, and c is the specific heat. Again, W_{st} is expressed in units of energy per unit surface area. The equivalent circuit (shown in figure 2) have resistances given by:

$$R_{cv} = \frac{1}{h} \qquad R_{rad} = \frac{1}{\epsilon\sigma(T_s^2 + T_{amb}^2)(T_s + T_{amb})} \qquad \text{and} \qquad R_{cnd} = \frac{1}{k}. \tag{6}$$

3 Thermophysical Algebraic Invariants, TAI's

The energy balance equation, $W_{abs} = W_{rad} + W_{cv} + W_{st} + W_{cnd}$ may be rewritten in the following linear form:

$$a_1 x_1 + a_2 x_2 + a_3 x_3 + a_4 x_4 + a_5 x_5 = \bar{\mathbf{a}}^T \bar{\mathbf{x}} = 0. \tag{7}$$

Using the expressions for the various energy components as presented in the previous section we can express each term in the above expression as:

$$\begin{aligned} a_1 &= C_T & x_1 &= -\tfrac{dT_s}{dt} \\ a_2 &= k & x_2 &= -\tfrac{dT_s}{dx} \\ a_3 &= -(T_s - T_{amb}) & x_3 &= h \\ a_4 &= -\sigma\ (T_s^4 - T_{amb}^4) & x_4 &= \epsilon \\ a_5 &= cos\theta_I & x_5 &= W_I \alpha_s \end{aligned} \tag{8}$$

Note that a calibrated LWIR image provides radiometric temperature. However, this requires knowledge of the emissivity, ϵ, of the surface. For common outdoor materials, and common paints and surface coatings, the value of ϵ is around 0.9 [25],[26]. Therefore, the radiometric temperature, T_s, may be computed based on the assumption, $\epsilon = 0.9$. Hence a_3 and a_4 can be computed from the LWIR image alone (and knowledge of the ambient temperature), while a_1, a_2 and a_5 are known when the identity and pose of the object is hypothesized. The "driving conditions", or unknown scene parameters that can change from scene to scene are given by the x_i, $i = 1, \ldots, 5$. Thus each pixel in the thermal image eqn (8) defines a point in 5-D thermophysical space.

Consider two different LWIR images of a scene obtained under different scene conditions and from different viewpoints. For a given object, N points are selected such that (a) the points are visible in both views, and (b) each point lies on a different component of the object which differs in material composition and/or surface orientation. Assume (for the nonce) that the object pose

for each view, and point correspondence between the two views are available (or hypothesized). A point in each view yields a measurement vector $\bar{\mathbf{a}} = (a_1, a_2, a_3, a_4, a_5)^T$ with components defined by eqn (8) and a corresponding driving conditions vector $\bar{\mathbf{x}} = (x_1, x_2, x_3, x_4, x_5)^T$. Let a collection of N of these vectors compose a $5 \times N$ matrix, $\mathbf{A} = (\bar{\mathbf{a}}_\mathbf{1}, \bar{\mathbf{a}}_\mathbf{2}, \ldots, \bar{\mathbf{a}}_\mathbf{N})$ for the first scene/image. These same points in the second scene will define vectors that compose a $5 \times N$ matrix, $\mathbf{A}' = (\bar{\mathbf{a}}'_\mathbf{1}, \bar{\mathbf{a}}'_\mathbf{2}, \ldots, \bar{\mathbf{a}}'_\mathbf{N})$. The driving condition matrix, $\mathbf{X} = (\bar{\mathbf{x}}_\mathbf{1}, \bar{\mathbf{x}}_\mathbf{2}, \ldots, \bar{\mathbf{x}}_\mathbf{N})^\mathbf{T}$, from the first scene and $\mathbf{X}' = (\bar{\mathbf{x}}'_\mathbf{1}, \bar{\mathbf{x}}'_\mathbf{2}, \ldots, \bar{\mathbf{x}}'_\mathbf{N})^\mathbf{T}$ from the second scene, are each of size $N \times 5$.

Since the N points are selected to be on different material types and/or different surface orientations, the thermophysical diversity causes the N vectors $\bar{\mathbf{a}}_\mathbf{1}, \bar{\mathbf{a}}_\mathbf{2}, \ldots, \bar{\mathbf{a}}_\mathbf{N}$ to span $\Re^5$, as will also the vectors, $\bar{\mathbf{a}}'_\mathbf{1}, \bar{\mathbf{a}}'_\mathbf{2}, \ldots, \bar{\mathbf{a}}'_\mathbf{N}$. Without loss of generality, assume that five vectors $\bar{\mathbf{a}}_\mathbf{1}, \ldots, \bar{\mathbf{a}}_\mathbf{5}$ span $\Re^5$ and also that $\bar{\mathbf{a}}'_\mathbf{1}, \ldots, \bar{\mathbf{a}}'_\mathbf{5}$ span $\Re^5$. These five points in $\Re^5$ specify the 5×5 measurement matrices, $\mathbf{A} = (\bar{\mathbf{a}}_\mathbf{1}, \bar{\mathbf{a}}_\mathbf{2}, \ldots, \bar{\mathbf{a}}_\mathbf{5})$, in the first scene and $\mathbf{A}' = (\bar{\mathbf{a}}'_\mathbf{1}, \bar{\mathbf{a}}'_\mathbf{2}, \ldots, \bar{\mathbf{a}}'_\mathbf{5})$, in the second scene. The point selection process here is analogous to the selection of characteristic 3D points in the construction of geometric invariants. Since $\mathbf{A}$ and $\mathbf{A}'$ are of full rank, there exists a linear transformation $S \in GL(5)$ such that $\mathbf{A} = S\mathbf{A}'$. Hence,

$$\bar{\mathbf{a}}_\mathbf{k} = S\bar{\mathbf{a}}'_\mathbf{k}, \quad k = 1, \ldots, 5 \tag{9}$$

Since from (7),

$$\bar{\mathbf{x}}_\mathbf{k}^T \bar{\mathbf{a}}_\mathbf{k} = \bar{\mathbf{x}}'^T_\mathbf{k} \bar{\mathbf{a}}'_\mathbf{k} = 0 \tag{10}$$

we have,

$$\begin{aligned} (\bar{\mathbf{x}}_\mathbf{k}^T S - \bar{\mathbf{x}}'_\mathbf{k})\bar{\mathbf{a}}'_\mathbf{k} = 0 \\ \bar{\mathbf{x}}'_\mathbf{k} = S^T \bar{\mathbf{x}}_\mathbf{k} \end{aligned} \tag{11}$$

Thus each driving condition vector also undergoes a linear transformation.

Consider the measurement vector $\bar{\mathbf{a}}$ of a point as defined in (8). From one scene to the next we expect the two object properties – thermal capacitance, C_T, and conductance, k – to remain

constant. Thus the transformation we need to consider is seen to be a subgroup of $GL(5)$ which has the form $M : \bar{\mathbf{a}} \rightarrow \bar{\mathbf{a}}'$ where,

$$M = \begin{bmatrix} 1 & 0 & 0 & 0 & 0 \\ 0 & 1 & 0 & 0 & 0 \\ m_{31} & m_{32} & m_{33} & m_{34} & m_{35} \\ m_{41} & m_{42} & m_{43} & m_{44} & m_{45} \\ m_{51} & m_{52} & m_{53} & m_{54} & m_{55} \end{bmatrix}. \tag{12}$$

The transformation of a measurement vector from one scene to the next is given by:

$$\begin{bmatrix} 1 & 0 & 0 & 0 & 0 \\ 0 & 1 & 0 & 0 & 0 \\ m_{31} & m_{32} & m_{33} & m_{34} & m_{35} \\ m_{41} & m_{42} & m_{43} & m_{44} & m_{45} \\ m_{51} & m_{52} & m_{53} & m_{54} & m_{55} \end{bmatrix} \begin{bmatrix} a_1 \\ a_2 \\ a_3 \\ a_4 \\ a_5 \end{bmatrix} = \begin{bmatrix} a'_1 \\ a'_2 \\ a'_3 \\ a'_4 \\ a'_5 \end{bmatrix}, j = 1, 2, \ldots, 5 \tag{13}$$

The first two elements, the thermal capacitance and the thermal conductance, are held constant and the other scene dependent elements are allowed to change. In general, we have $M\mathbf{A} = \mathbf{A}'$, where $\mathbf{A}$ and $\mathbf{A}'$ are the 5×5 matrices derived from the two scenes and for the chosen points.

Now that the transformation of the point configuration has been established in 5D thermophysical space, we ask the question - what function of the coefficients, $a_{i,j}$, is invariant to transformations of the form - equation (12)? In answer to this question we first determine the expected number of invariant relationships. The transformation group represented by M has 15 parameters. The measurement matrix A has 25 degrees of freedom. The counting argument described by Mundy [1] and others is that the number of invariant relationships is equal to "the degrees of freedom of the configuration" minus "the number of transformation parameters". Here a count yields 10 invariant relationships for a configuration of five points. However, the counting argument also shows us that it is unnecessary to use all five points. Each point has

five degrees of freedom. In order for invariant relationships to exist, a minimum of four points can be used. Using four points the counting argument gives $20 - 15 = 5$ independent invariant relations. Note that this further simplifies the point selection since we now require only four points in the two views. The measurement vectors in each view being required to span $\Re^4$.

Algebraic elimination of the transformation parameters using four copies of the linear form (7) subjected to the transformation (12) provides us with the invariants. This elimination may be performed by using recently reported symbolic techniques [27].

The five invariant functions derived by this elimination process can be divided into two types. Each is a ratio of determinants. Indeed, it is well known that absolute invariants of linear forms are always ratios of powers of determinants [28]. The first type of invariant function is a determinant formed from components of three of the four vectors.

$$I1 = \frac{\begin{vmatrix} a_{1,3} & a_{2,3} & a_{4,3} \\ a_{1,4} & a_{2,4} & a_{4,4} \\ a_{1,5} & a_{2,5} & a_{4,5} \end{vmatrix}}{\begin{vmatrix} a_{2,3} & a_{3,3} & a_{4,3} \\ a_{2,4} & a_{3,4} & a_{4,4} \\ a_{2,5} & a_{3,5} & a_{4,5} \end{vmatrix}} \tag{14}$$

where $a_{i,j}$ is a jth component of the ith vector (ith point).

The second type is formed from components of all four vectors.

$$I2 = \frac{\begin{vmatrix} a_{1,1} & a_{2,1} & a_{3,1} & a_{4,1} \\ a_{1,2} & a_{2,2} & a_{3,2} & a_{4,2} \\ a_{1,4} & a_{2,4} & a_{3,4} & a_{4,4} \\ a_{1,5} & a_{2,5} & a_{3,5} & a_{4,5} \end{vmatrix}}{\begin{vmatrix} a_{1,1} & a_{2,1} & a_{3,1} & a_{4,1} \\ a_{1,3} & a_{2,3} & a_{3,3} & a_{4,3} \\ a_{1,4} & a_{2,4} & a_{3,4} & a_{4,4} \\ a_{1,5} & a_{2,5} & a_{3,5} & a_{4,5} \end{vmatrix}} \tag{15}$$

where $a_{i,j}$ is a jth component of the ith vector (ith point). Since the 4 measurement vectors span $\Re^4$, we can assume without loss of generality that the denominator determinants in (14) and (15) are non-zero. The number of independent functions that can be formed with four points must add up to the expected number from the counting argument. The first type has $\begin{pmatrix} 4 \\ 3 \end{pmatrix} = 4$, independent functions given four points and second type has one. The counting argument is thus satisfied.

The derivation of thermophysical algebraic invariant features, as described above, relies on a number of assumptions. These assumptions are summarized. (1) Four points are chosen such that measurement vectors (in each scene) are linearly independent, i.e. one (or more) of the four points have different material properties and/or surface normal. (2) The four points are related by a linear transformation of the form (12) from one scene to another. (3) The points are corresponded. (4) Object identity is hypothesized (which is verified or reputed by the feature value). (5) The thermal capacitance and conductance of the object (surface) do not change while other other scene variable are allowed to vary from one scene to another. (6) Emissivity of the imaged surface in the $8\mu m - 12\mu m$ band is 0.9. The first two assumptions go

hand in hand, the vectors are linearly independent by proper choice of the points, i.e. model formation. Most objects have sufficient diversity in surface material types to easily satisfy this requirement. Given such proper model formation, the existence of linear transformation M is trivially ensured. The point correspondence and the hypothesis assumptions are satisfied in the method of application of the features, described in section 3.1. Assumption (6) is satisfied except for bare metal surfaces and esoteric low emissivity coatings.

In order for the invariant feature to be useful for object recognition not only must the values of the feature, be invariant to scene conditions but the value must be different if the measurement vector is obtained from a scene that does not contain the hypothesized object, and/or if the hypothesized pose is incorrect. Since the formulation above takes into account only feature invariance but not separability, a search for the best set of points that both identifies the object and separates the classes must be conducted over a given set of points identified on the object. The search may be conducted over all the combination of the points in a set or until an acceptable feature is found. We have examined all combinations, first rating each set for their intra-class invariance, then further evaluating it for inter-class separability. Results on real imagery are described in section 5.

3.1 Employing TAI's for Object Recognition

The feature computation scheme formulated above is suitable for use in an object recognition system that employs a hypothesize-and-verify strategy. The scheme would consist of the following steps: (1) extract geometric features, e.g., lines and conics, (2) for image region, r, hypothesize object class, k, and pose using, for example, geometric invariants as proposed by Forsyth, et al [2], (3) use the model of object k and project visible points labeled $i = 1, 2, \ldots$ onto image region r using scaled orthographic projection, (4) for point labeled i in the image

region, assign thermophysical properties of point labeled i in the model of object k, (5) using gray levels at each point and the assigned thermophysical properties, compute the measurement matrices A and A', and hence compute the feature $f^k(r)$ using equation (14) or equation (15), and finally, (6) compare feature $f^k(r)$ with model prototype $\hat{f}_k$ to verify the hypothesis.

For example, consider two class of vehicles - a van and a car as shown in figure 3. Here, the correct hypotheses (models) are shown in the top row. The bottom row indicate incorrect hypotheses with model points being assigned to the image regions. The front and rear wheels are detected and used to establish an object centered reference frame in the image to be interpreted. The coordinates of the selected points are expressed in terms of this 2D object centered frame. Thus, when a van vehicle is hypothesized for an image actually obtained of a car or some unknown vehicle, the material properties of the van are used, but image measurements are obtained from the image of the car at locations given by transforming the coordinates of the van points (in the van center coordinate frame) to the image frame computed for the unknown vehicle.

4. Varying Contextual Support

It is widely known that the explicit use of contextual knowledge can improve scene interpretation performance. Such contextual knowledge has been, typically, in the form of spatial and geometric relationships between scene objects or between different components of an object. Contextual support for an image region (point) being labeled consists of the neighboring regions (points), the class memberships of which influence the class assignment for the region (point) under consideration. In the feature extraction scheme described in section 3, contextual knowledge is used in an implicit manner. Recall that a set of points is hypothesized to belong to a specific type of object, and this hypothesis is verified. Thus, the class identity of each of

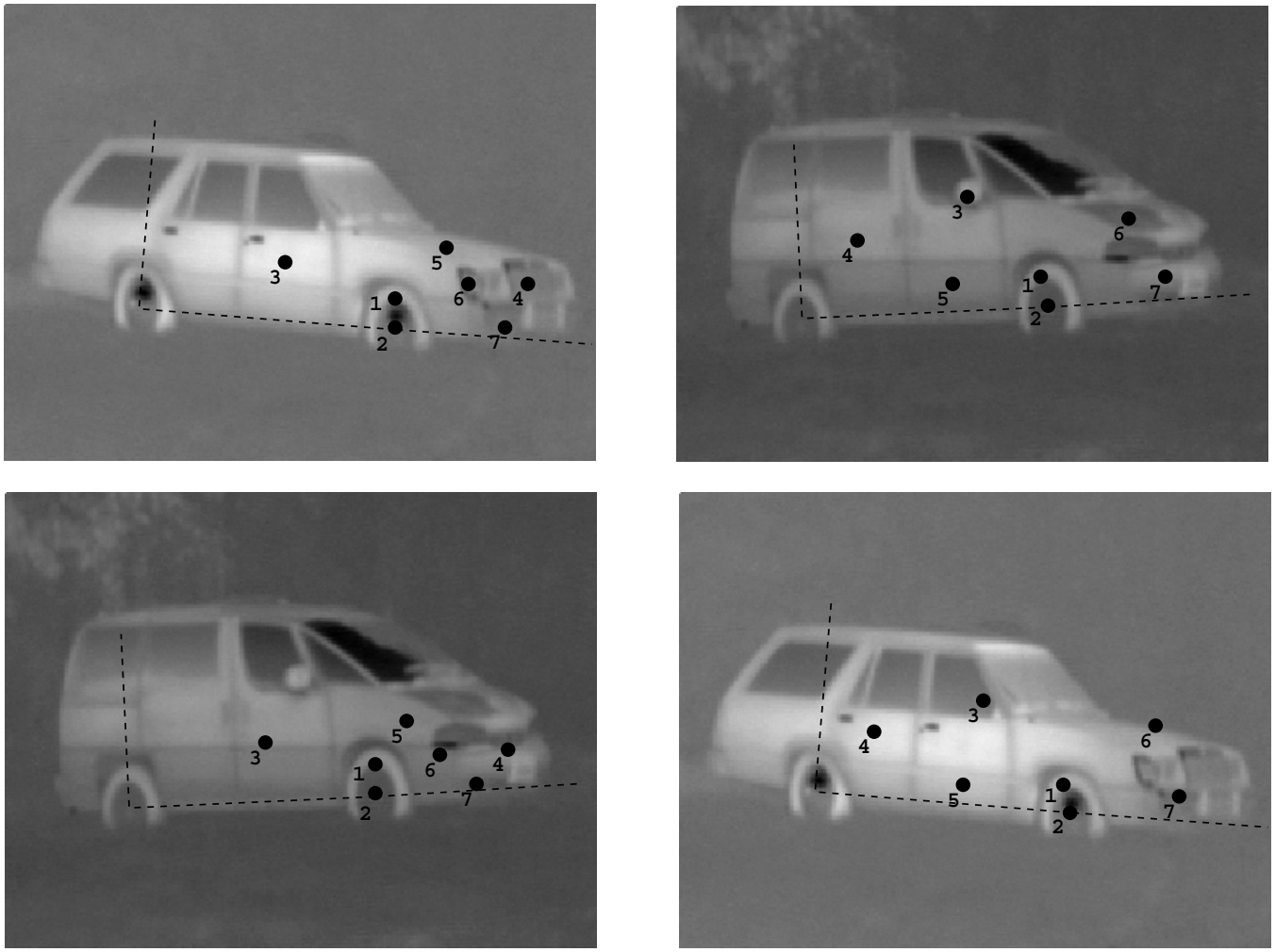

Figure 3: **Top row –** the car and van object types with points selected on the surface with different material properties and/or surface normals. For the van – Point 1: Vulcanized Rubber, 2: Aluminum Alloy, 3: Polystyrene-like polymer, 4: Steel, 5: Polypropylene-like polymer, 6: Steel, 7: Polypropylene-like polymer For the car – Point 1: Vulcanized Rubber, 2: Steel, 3: Steel, 4: Chromed Steel, 5: Steel, 6: Polycarbonate, 7: Carbon Steel. **Bottom row –** assignment of point labels under erroneous hypotheses. First, the two wheels of the vehicle are used to establish a local, 2D, object-centered coordinate frame. Then, the 2D to 2D transformation between model and image is determined, and the model points and labels are transformed to the image.

these points is made in the context of the identities of the other points.

The computation of feature $I2$ described in section 3 requires 4 points while the computation of $I1$ requires only 3 points. Thus, $I1$ and $I2$ require different amounts of contextual support. In some situations the available, useful, contextual support may be even lower, since it may be possible to extract only one or two points reliably, e.g., where the object is partially occluded or if the specific aspect view contains only a homogeneous surface. The formulation of feature $I1$ does allow for this reduction in contextual support as explained below.

The variation in context may also be viewed as a variation in the dimensionality of a specific predetermined subspace of the thermophysical feature space. The dimensionality of the subspace determines the number of measurements required from the thermal image, and hence the degree of context used. As the number of image measurements is increased, fewer dimensions are required in the precomputed subspace and more context is derived from the imaged object. In the method presented below, a subspace in thermophysical measurement space is precomputed for each invariant feature established for an object class.

Consider the formulation of feature $I1$ which can be expressed in the form

$$f = \frac{|\bar{\mathbf{b}}_1 \bar{\mathbf{b}}_2 \bar{\mathbf{b}}_3|}{|\bar{\mathbf{b}}_1 \bar{\mathbf{b}}_2 \bar{\mathbf{b}}_4|} \tag{16}$$

$$= \frac{|B|}{|\hat{B}|} \tag{17}$$

where the column vectors $\bar{\mathbf{b}}_\mathbf{i}$ that compose $\hat{B}$ span $\Re^3$. For non-zero invariants, the column vectors $\bar{\mathbf{b}}_\mathbf{i}$ that compose B also span $\Re^3$. In the above, we have $n+1$ points in an n-D space, where $n = 3$. The points are divided into two sets each consisting of n points, and the two sets differ by one element, and share $n-1$ common points.

The measurement matrices in (16) may be expressed, in general, as: $B = [\bar{\mathbf{b}}_\mathbf{1} \ \ldots \ \bar{\mathbf{b}}_\mathbf{n-1} \ \bar{\mathbf{b}}_\mathbf{n}]$ and $\hat{B} = [\bar{\mathbf{b}}_\mathbf{1} \ \ldots \ \bar{\mathbf{b}}_\mathbf{n-1} \ \bar{\mathbf{b}}_\mathbf{n+1}]$. Consider $\vec{\eta}$, which spans the null space of $B^* = [\bar{\mathbf{b}}_\mathbf{1} \ \ldots \ \bar{\mathbf{b}}_\mathbf{n-1}]$, i.e. $B^*\vec{\eta} = 0$. Note that $B^* = [\bar{\mathbf{b}}_\mathbf{1}\bar{\mathbf{b}}_\mathbf{2}]$, for $n = 3$. The feature value, $\frac{|B|}{|\hat{B}|}$, is non-infinite and

non-zero if and only if $\bar{\mathbf{b}}_{\mathbf{n}}^{\mathbf{T}}\vec{\eta} \neq 0$ and $\bar{\mathbf{b}}_{\mathbf{n+1}}^{\mathbf{T}}\vec{\eta} \neq 0$. Furthermore, it can be shown that:

$$\frac{|B|}{|\hat{B}|} = \frac{\bar{\mathbf{b}}_{\mathbf{n}}^{\mathbf{T}}\vec{\eta}}{\bar{\mathbf{b}}_{\mathbf{n+1}}^{\mathbf{T}}\vec{\eta}} \tag{18}$$

The proof of this statement is included in appendix A.

For convenience of terminology, let us call the vector $\vec{\eta}$ the null-space vector. The components of the null-space vector can be found by,

$$\frac{\bar{\mathbf{b}}_{\mathbf{n}}^{\mathbf{T}}\vec{\eta}}{\bar{\mathbf{b}}_{\mathbf{n+1}}^{\mathbf{T}}\vec{\eta}} = f, \qquad \bar{\mathbf{b}}_{\mathbf{n}}^{\mathbf{T}}, \bar{\mathbf{b}}_{\mathbf{n+1}}^{\mathbf{T}}, \vec{\eta} \in \Re^n; \tag{19}$$

$$(\bar{\mathbf{b}}_{\mathbf{n}} - f\bar{\mathbf{b}}_{\mathbf{n+1}})^T\vec{\eta} = 0 \tag{20}$$

Consider instances of the null-space vector defined above for different scene conditions. Each scene condition, in which the object is imaged, results in a different null space vector $\vec{\eta}(j)$ where, $j = 1, 2, \ldots$. For a given object, it may be possible to find a collection of $n+1$ points and a decomposition into two sets of n points each such that the corresponding the null-space vectors, $\vec{\eta}(j)$, for the different scenes are tightly clustered in the measurement space, i.e., they vary minimally from scene to scene. If this condition is met it is reasonable to use a single predetermined average null-space vector, $\vec{\eta}^*$, that characterizes the object irrespective of the scene conditions. Now, only two measurement vectors, $\bar{\mathbf{b}}_{\mathbf{n}}$ and $\bar{\mathbf{b}}_{\mathbf{n+1}}$ are needed to compute the invariant feature - using the image and hypothesized object class, as described in section 3. Equation (19) becomes,

$$\frac{\bar{\mathbf{b}}_{\mathbf{n}}^{\mathbf{T}}\vec{\eta}^*}{\bar{\mathbf{b}}_{\mathbf{n+1}}^{\mathbf{T}}\vec{\eta}^*} = f^*, \tag{21}$$

where f^* is the feature value obtained using the average (representative) null-space vector.

In general, one needs to search (during a training phase) for an appropriate set of $n+1$ points, and a decomposition of this set into two sets of n points each that share $n-1$ points, with the constraint that the null space vectors vary minimally from scene to scene. This will establish the optimal two-point invariants for the object.

In order for the null-space vector approach to be useful in an object recognition scheme, separability between the object classes must be ensured. That is, for the correct object hypothesis, the feature value given by equation (21) must be as expected and must remain invariant to scene conditions while in the case that the object hypothesis is erroneous a value other than the expected invariant feature value is obtained. Consider a two-class separation problem. The null-space vectors from different scenes for each object will ideally form a tight cluster. Separability between these clusters can be measured using any of the many established statistical measures, e.g. the *Mahalanobis distance* [29].

The variation in contextual support offered by the above methods may be exploited in a hierarchal system where the two-point formulation is used for a quick, initial classification, with low missed detection rate but perhaps high false alarm rate, to eliminate fruitless branches in a broad search tree. In the following section we present results illustrating the classification ability of the method described in section 3 as well as that of the null-space vector approach for multiple objects.

4 Experimental Results

The method of computing thermophysical affine invariants discussed above was applied to real LWIR imagery acquired at different times of the day. Several types of vehicles were imaged: A van containing mostly plastic (composite) body panels, a car made entirely of sheet-metal body panels, a military tank, and two different military trucks (Figs. 3,4). Several points were selected (as indicated in the figures) on the surfaces of different materials and/or orientation. The measurement vector given by eqn (8) was computed for each point, for each image/scene.

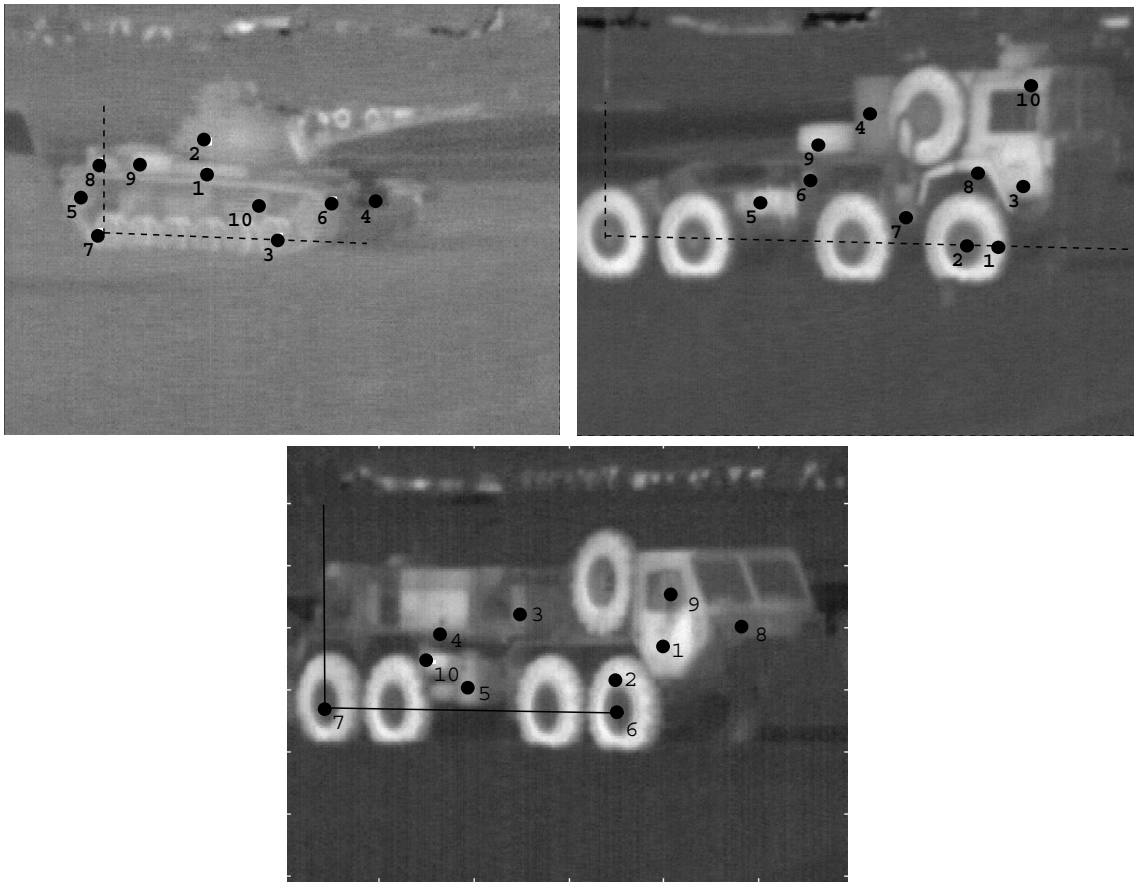

Figure 4: Three of the vehicles used to test the object recognition approach, (from top left clockwise) tank, truck 1 and truck 2. The axis superimposed on the image show the object centered reference frames. The numbered points indicate the object surfaces used to form the measurement matrices. These points are selected such that there are a variety of different materials and/or surface normals within the set.

Hypothesis: Data From:	Truck 1 Truck 1	Truck 1 Tank	Truck 1 Van	Truck 1 Car	Truck 1 Truck 2
11 am	-0.70	27.28	0.33	$-\infty$	0.68
12 pm	-0.71	0.09	4.83	15.58	4.15
1 pm	-0.45	0.68	0.00	11.73	4.6e12
2 pm	-0.66	-1.00	$-\infty$	71.23	-1.00
3 pm	-0.40	-1.00	$-\infty$	-1.00	-1.00
4 pm	-0.54	$-\infty$	∞	5.42	22.29
9 am	-0.68	1.38	-1.00	-6.66e14	-7.03
10 am	-0.45	-1.00	$-\infty$	6.50	∞

Table 1: Values of the I1-type feature used to the identify the vehicle class, truck 1. The feature consisted of point set $\{4, 7, 8, 10\}$, corresponding to the points labeled in figure 6. The feature value is formed using the thermophysical model of truck 1 and the data from the respective other vehicles. When this feature is applied to the correctly hypothesized data of the tank it has a mean value of -0.57 and a standard deviation of 0.13. This I1-type feature produces a good stability measure of 4.5, and good separability between correct and incorrect hypotheses. The feature values for incorrect hypotheses are at least 3.32 standard deviations away from the mean value for the correct hypothesis.

Hypothesis: Data From:	Truck 1 Truck 1	Truck 1 Van	Truck 1 Car	Truck 1 Tank	Truck 1 Truck 2
11 am	-0.16	-193.47	-60.39	59.78	∞
12 pm	-0.28	-387.66	-143.09	20.20	∞
1 pm	-0.09	-525.77	-150.70	-11.23	-1.01e5
2 pm	-0.48	∞	-39.01	-29.38	1.02e5
3 pm	-0.96	-79.45	-1.7e5	-80.83	5.2e5
4 pm	-1.42	-498.51	50.76	∞	∞
9 am	-0.31	-454.87	-252.78	-9.38	29.9e5
10 am	-0.20	-13.90	-240.88	-7.78	∞

Table 2: Values of the I2-type feature used to the identify truck 1. The feature consisted of point set $\{2, 3, 5, 9\}$, corresponding to the points labeled in figure 4. The feature value is formed using the thermophysical model of truck 1 and the data from the respective other vehicles. When this feature is applied to the correctly hypothesized data of truck 1 it has a mean value of -0.49 and a standard deviation of 0.46. The feature values under an incorrect hypothesis are at least 15.2 standard deviations away from the mean value for the correct hypothesis.

Given N points on the object to form the feature of type $I1$, or of type $I2$, there are

$$n_N = \begin{pmatrix} N \\ 4 \end{pmatrix} \begin{pmatrix} 4 \\ 3 \end{pmatrix} \tag{22}$$

Each of the n_N features have a distribution of values from scene to scene. The non-zero variance is due to many factors including: (a) how well the linear thermophysical model is satisfied, (b) calibration errors, and (c) numerical computation errors. In our experiments the features were computed for all the combinations of points for the different scenes. A large number of four-point-sets yielded features with low variance from scene to scene. First, the point sets were rated based on their stability/low variance, where the stability is defined as the average value of the feature over time, divided by the standard deviation of the feature for that time period. Next, the most stable features were evaluated for inter-class separation as explained below.

As mentioned in section 3 the feature is computed based on the hypothesized identity of the object (and it's thermophysical properties). Hence, if the object identity (class membership) k is hypothesized in the image region r, then the image measurements are used along with the thermophysical properties of object class k to generate a feature value $f^k(r)$. Verification of this hypothesis may be achieved by comparing $f^k(r)$ with a class prototype $\hat{f}^k$. This comparison may be achieved using any of a number of available classifier rules, e.g., minimum distance rule. Since it is important that erroneous hypotheses be refuted, one must consider inter-class behavior as well as intra-class behavior of the feature. To experimentally investigate such behavior using real imagery we adopted the following procedure. Given an image of a vehicle, (1) assume the pose of the vehicle is known, then (2) use the front and rear wheels to establish an object centered reference frame. The center of the rear wheel is used as the origin, and center of the front wheel is used to specify the direction and scaling of the axes. The coordinates of the selected points are expressed in terms of this 2D object centered frame. For example, when a van vehicle is hypothesized for an image actually obtained of a car or some unknown vehicle,

the material properties of the van are used, but image measurements are obtained from the image of the car at locations given by transforming the coordinates of the van points (in the van center coordinate frame) to the image frame computed for the unknown vehicle.

Table 1 shows inter-class and intra-class variation for a feature of type $I1$ for the truck 1 object class – for images obtained at eight different times over two days. The behavior of the invariant feature formed by one choice of a set of 4 points is shown in table 1 for correct hypothesis. Also, table 1 shows the case where the hypothesized object is the truck 1 while the imaged object is either a car, van, truck 2, or tank. As can be seen, the correct hypothesis generates a feature value that is invariant and distant from the feature values generated by erroneous hypotheses. Thus, the feature is shown to have good characteristics in both (high) inter-class separability and (low) intra-class stability. Table 2 shows similar results for a feature of type $I2$ also used for separating truck 1 from other objects. Table 3 describes the performance of a feature of type $I2$ used to separate the tank object class from other classes. Features for each of the other object classes were also examined, and performance similar to that described above was observed. Also, each class produced a large number of features (of each type) that demonstrated good inter-class separation and intra-class stability.

The method described in section 4 was used to compute two-point invariant features for the 5 types of classes examined above. The ten points chosen on the truck 1 vehicle corresponding to the points in Fig. 4 provide 210 different features. For each selection of a pair of points, the average null vector is computed over different images under the correct hypothesis. This vector is then used to compute the feature under mistaken hypotheses. The ability of this feature to separate correct hypotheses from mistaken hypotheses can be described by the measure

$$\mathcal{P} = \frac{|\mu_c - \mu_m|}{\sigma_c \sigma_m},$$

where μ_c and μ_m are the mean values for the correct hypothesis and mistaken hypothesis, respectively, and σ_c and σ_m are the corresponding standard deviations [30]. The performance

Hypothesis: Data From:	Tank Tank	Tank Van	Tank Car	Tank Truck 1	Tank Truck 2
11 am	0.88	-648.99	∞	∞	25.37
12 pm	0.88	198.98	∞	-38.19	-9.47
1 pm	1.29	-339.60	∞	∞	-7.68
2 pm	3.25	-154.42	-6.55	∞	-7.31
3 pm	4.12	-290.50	-12.48	∞	-7.84
4 pm	2.60	-339.92	-20.41	∞	∞
9 am	1.07	-2.42e5	∞	-13.19	-5.31
10 am	0.70	∞	∞	-4.64	-3.57

Table 3: Values of a feature of type $I2$ used to the identify the tank, for correct and mistaken hypothesis. The feature consisted of point set $\{3, 5, 7, 9\}$, corresponding to the points labeled in figure 4. The feature value is formed using the thermophysical model of tank and the data from the respective other vehicles. When this feature is applied to the correctly hypothesized data of the tank it has a mean value of 2.52 and a standard deviation of 1.82. The feature value under a mistaken hypothesis is at least 3.3 standard deviations away from the average value under the correct hypothesis.

Hypothesis: Data From:	Truck 1 Tank	Truck 1 Van	Truck 1 Car	Truck 1 Truck 2
Feature 1:	78.13	14.89	3.55	9.33
Feature 2:	75.72	13.01	3.30	7.25
Feature 3:	29.46	6.46	3.29	6.97
Feature 4:	24.98	5.62	3.23	6.81
Feature 5:	16.29	5.42	3.02	5.86

Table 4: Separability measure for the two-point features derived in section 4. The features were derived for separating the class Truck 1 from other classes. Larger values indicate better separation between correct hypotheses and erroneous ones.

of the best five features identified for the truck 1 object class is given in table 4. Similar features are available for the other object classes.

5 Discussion

The approach described above is promising in that it makes available features that are (1) invariant to scene conditions, (2) able to separate different classes of objects, and (3) based on physics based models of the many phenomena that affect LWIR image generation.

It is important to note that although the derivation of the features explicitly used the constraint that the value be invariant from one scene to another for a given object class, class separation was not explicitly incorporated in the derivation of the features. Hence, practical use of the approach for recognition requires searching all the possible features for the best separation. It is not clear that a solution will always exist for a collection of object classes. Note that different aspects of an object may be imaged – the set of visible points being different for each aspect. The complexity of the search task is compounded by attempting to ensure inter-class separation in the presence of erroneous pose hypothesis, which we have not considered in this paper.

The hypothesis of object pose and identity is best achieved by employing geometrical invariance techniques [2]. For example, conics may be fit to wheels which manifest high contrast in LWIR imagery, and their parameter values may be used to compute GI's. This may be employed to generate object identity and pose that may be verified by the thermophysical invariance scheme described above. This approach is also being investigated at present.

Note that the formulation described in this paper assumes that the scene objects are passive, i.e., internal thermal sources are not explicitly modeled. The experiments were conducted on

vehicles that had not been exercised prior to (or during) image acquisition. Reformulation of the scheme presented in this paper to explicitly incorporate internal sources will be a interesting area of future research.

The specification of optimal classifiers that use as input the features established in this paper is another area that merits investigation. In our experiments, we have found that the distribution of the features, especially under erroneous hypotheses, are poorly modeled by the commonly used Gaussian distribution. We are investigating the use of Symmetric Alpha Stable Distributions which appear to model the behavior of the features more closely. Our research in this area is directed at realizing classifiers with low false alarm rates and high detection probabilities that use features based on the the above physics based approach for a variety of applications.

6 Acknowledgments

The authors thank Tushar Saxena and Deepak Kapur of the Institute for Logic and Programming, Computer Science Dept, State University of New York at Albany, for making available to us their algorithmic elimination methods. This research was supported by the AFOSR contract F49620-93-C-0063, the AFOSR grant LRIR-93WL001, an AFOSR Laboratory Graduate Fellowship, ARPA contract F33615-94-C-1529 and the National Science Foundation Contract IRI-91109584.

References

[1] Mundy, J. , Zisserman, A., editors, *Geometric Invariance in Computer Vision*, The MIT Press, 1992.

[2] D. Forsyth, J.L. Mundy, A. Zisserman, C. Coelho, A. Heller, C. Rothwell, "Invariant Descriptors for 3D Object Recognition and Pose", *IEEE Trans PAMI*, vol 13, no 12, Oct 1991

[3] T. Binford, T.S. Levitt, and W.B. Mann, "Bayesian Inference in Model-Based Vision", *Uncertainty in AI, 3*, L.N. Kanal, T.S. Levitt, and J.F. Lemmer, (Ed's), Elsevier, 1989.

[4] J.B. Burns, R.S. Weiss, and E.M. Riseman, "View Variation of Point-Set and Line-Segment Features", *IEEE Trans PAMI*, vol 15, no 1, Jan 1993.

[5] T.H. Reiss, "Recognizing Planar Objects Using Invariant Image Features", *Lecture Notes in Computer Science, 676,* G. Goos and J. Hartmanis (Eds), Springer-Verlag, Berlin, 1993.

[6] E. Rivlin and I. Weiss, "Semi-Local Invariants", *Proc IEEE CVPR* 1993, pp. 697-698

[7] D. Weinshall, "Direct Computation of Qualitative 3D Shape and Motion Invariants", *IEEE Trans PAMI*, vol 13, no 12, Dec 1991.

[8] D. Weinshall, "Model-based Invariants for 3D Vision", *Proc IEEE CVPR* 1993, pp. 695-696

[9] I. Weiss, "Noise-Resistant Invariants of Curves", *IEEE Trans PAMI*, vol 15, no 9, July 1993, pp. 943-948

[10] M. Zerroug and R. Nevatia, "Quasi-Invariant Properties and 3D Shape Recovery of Non-Straight, Non-Constant Generalized Cylinders", *Proc IEEE CVPR 1993*, pp 96-103

[11] L.B. Wolff, "Polarization-based material classification from specular reflection", *IEEE Trans PAMI*, Nov 1990, pp 1059-1071.

[12] J. Koenderink and A.J. van Doorn, "Photometric Invariants Related to Solid Shape", *Optica Acta*, Vol. 27, No. 7, 1980, pp. 981-996.

[13] A. Blake, A. Zisserman, and G. Knowles, "Surface Descriptions from Stereo and Shading", *Image and Vision Computing*, Vol. 3, No. 4, 1985, pp. 183-191.

[14] L.B. Wolff and E. Angelopoulou, "3-D Stereo Using Photometric Ratios", *Proceedings of the Third European Conference on Computer Vision* Stockholm Sweden, May 1994 pp. 247-258.

[15] G. Healey and D. Slater, "Using Illumination Invariant Color Histogram Descriptors for Recognition", *Proc IEEE Conf CVPR*, June 21-24, 1994, Seattle, WA, pp. 355-360.

[16] S.K. Nayar and R.D. Bolle, "Reflectance Ratio: A Photometric Invariant for Object Recognition", *Proc IEEE ICCV*, 1993.

[17] M.J. Gauder, V.J. Velten, L.A. Westerkamp, J. Mundy, and D. Forsyth, "Thermal Invariants for Infrared Target Recognition", *ATR Systems and Technology Conf*, 1993.

[18] D.G. Lowe, "The Viewpoint Consistency Constraint," *International Journal of Computer Vision*, vol. 1, no. 1, 1987, pp. 57-72.

[19] N. Nandhakumar and J.K. Aggarwal, "Integrated Analysis of Thermal and Visual Images for Scene Interpretation", *IEEE Trans. on Pattern Analysis and Machine Intelligence*, Vol. 10, No. 4, July 1988, pp. 469-481.

[20] N. Nandhakumar, "A Phenomenological Approach to Multisource Data Integration: Analyzing Infrared and Visible Data", *Proc. IAPR TC7 Workshop on Multisource Data Integration in Remote Sensing,* College Park, MD, June 14-15, 1990.

[21] N. Nandhakumar and J.K. Aggarwal, "Thermal and Visual Information Fusion for Outdoor Scene Perception", *Proc. of IEEE International Conference on Robotics and Automation*, Philadelphia, PA, April 1988, pp. 1306-1308.

[22] N. Nandhakumar, "Robust Physics-based Sensor Fusion", Journal of the Optical Society of America, JOSA-A, 1994, to appear.

[23] F.P. Incropera and D.P. DeWitt, *Fundamentals of Heat Transfer*, John Wiley and Sons, New York, 1981.

[24] S.B. Idso and R.D. Jackson, "Thermal Radiation," *Geophysical Research*, 82(28), September 1977.

[25] Y.S. Toloukian, D.P. De Witt, and R.S. Hernicz, Eds, *Thermal Radiative Properties of Coatings*, Thermophysical Properties of Matter, vol. 9, Thermophysical Properties Research Center of Purdue University, Data Series, Plenum Publishing Corp., N.Y., 1972

[26] Y.S. Toloukian and C.Y. Ho, Eds, *Thermal Radiative Properties of Nonmetallic Solids*, Thermophysical Properties of Matter, vol. 8, Thermophysical Properties Research Center of Purdue University, Data Series, Plenum Publishing Corp., N.Y., 1972

[27] Kapur, D., Lakshman, Y.N. and Saxena, T., "Computing Invariants using Elimination Methods," Proc. *IEEE International Symposium on Computer Vision*, Coral Gables, Florida, Nov 21-23, 1995, pp 97-102.

[28] G.B. Gurevich, "Foundations of the Theory of Algebraic Invariants", (translated by J.R.M. Raddock and A.J.M. Spencer) P. Noordhoff Ltd - Groningen, The Netherlands, 1964

[29] P.C. Mahalanobis, "On the Generalized Distance in Statistics," *Proc. Nat. Inst. Sci. Calcutta*, Vol. 12, 1936 pp 49-55.

[30] K. Fukunaga, *Introduction to Statistical Pattern Recognition,* 2nd edition, Acedemic Press Ltd, London, UK.

Appendix A

From section 4 equation 18, the n-dimensional measurement matrices B and B' consist of $n-1$ common tensors. Each has one distinct vector. By projecting the distinct vectors onto the null space vector formed by the common vectors we find that the ratio of the projections is equivalent to the ratio of the determinants of the matrices.

Claim:

$$\frac{|B_{n\times n}|}{|B'_{n\times n}|} = \frac{b_n \cdot \vec{n}}{b'_n \cdot \vec{n}} \tag{23}$$

where $B'_{n\times n} = B_{n\times n}|_{b_n \to b'_n}$. The row vector b_n is $(1 \times n)$. The vector $\vec{n}$ has dimension $(n \times 1)$ and is formed with the submatrix $B_{n-1,n}$ by:

$$B_{n-1,n} \cdot \vec{n} = 0 \tag{24}$$

The entries of the A and A' matrices will be labeled:

$$B_{n\times n} = \begin{bmatrix} b_{1,1} & \dots & b_{1,n} \\ \vdots & & \vdots \\ b_{n,1} & \dots & b_{n,n} \end{bmatrix} B'_{n\times n} = \begin{bmatrix} b_{1,1} & \dots & b_{1,n} \\ \vdots & & \vdots \\ b'_{n,1} & \dots & b'_{n,n} \end{bmatrix} \tag{25}$$

Proof: Consider the determinants of 23 expanded along the last the row:

$$\frac{|B_{n\times n}|}{|B'_{n\times n}|} = \frac{b_{n,1}C_{n,1} + b_{n,2}C_{n,2} + \ldots + b_{n,n}C_{n,n}}{b'_{n,1}C_{n,1} + b'_{n,2}C_{n,2} + \ldots + b'_{n,n}C_{n,n}} \tag{26}$$

where $C_{j,k} = (-1)^{jk}M_{j+k}$, M_{jk} is the minor of b_{jk} in $|B_{n\times n}|$. Here $j = n$.

Now consider the null space vector, $\vec{n}$, formed by the submatrix $B_{n-1,n}$.

$$\begin{bmatrix} b_{1,1} & \dots & b_{1,n} \\ \vdots & & \vdots \\ b_{n-1,1} & \dots & b_{n-1,n} \end{bmatrix} \begin{bmatrix} n_1 \\ \vdots \\ n_{n-1} \\ 1 \end{bmatrix} = 0. \tag{27}$$

This leads to the system of equations,

$$\begin{array}{ccccccccc} b_{1,1}n_1 & + & b_{1,2}n_2 & + & \dots & + & b_{1,n-1}n_{n-1} & = & -b_{1,n} \\ \vdots & & \vdots & & & & \vdots & & \vdots \\ b_{n-1,1}n_1 & + & b_{n-1,2}n_2 & + & \dots & + & b_{n-1,n-1}n_{n-1} & = & -b_{n-1,n} \end{array} \tag{28}$$

Solving for the components of $\vec{n}$ by Cramers rule:

$$n_1 = \frac{D_1^*}{D_n^*}, \quad n_2 = \frac{D_2^*}{D_n^*}, \quad \ldots, \quad n_{n-1} = \frac{D_{n-1}^*}{D_n^*}. \tag{29}$$

where D_n^* is the determinant of the $(n-1 \times n-1)$ matrix of coefficients and D_i^* is the $(n-1 \times n-1)$ determinant formed by replacing the ith column in the matrix of coefficients by the vector of the right-hand-side values.

Expanding the dot product, substituting equation 29 and multiplying the numerator and denominator by D_n^* yields:

$$\frac{b_n \cdot \vec{n}}{b'_n \cdot \vec{n}} = \frac{b_{n,1}D_1^* + b_{n,2}D_2^* + \ldots + b_{n,n}D_n^*}{b'_{n,1}D_1^* + b'_{n,2}D_2^* + \ldots + b'_{n,n}D_n^*} \tag{30}$$

Comparing equation 26 with equation 30 shows that in order to establish the proof it is sufficient to show that the corresponding matrices are equal,

$$D_i^* = C_{n,i}. \tag{31}$$

From equation 26 $C_{n,1}$ is the cofactor of the $b_{n,i}$ element in $B_{n\times n}$. It is equal to:

$$C_{n,i} = \begin{bmatrix} b_{1,1} & \ldots & b_{1,i-1} & b_{1,i+1} & \ldots & b_{1,n-1} & b_{1,n} \\ \vdots & & \vdots & \vdots & & \vdots & \vdots \\ b_{n-1,1} & \ldots & b_{n-1,i-1} & b_{n-1,i+1} & \ldots & b_{n-1,n-1} & b_{n-1,n} \end{bmatrix} \tag{32}$$

The D_i^* matrix is

$$D_i^* = \begin{bmatrix} b_{1,1} & \ldots & b_{1,i-1} & -b_{1,n} & b_{1,i+1} & \ldots & b_{1,n-1} \\ \vdots & & \vdots & \vdots & \vdots & & \vdots \\ b_{n-1,1} & \ldots & b_{n-1,i-1} & -b_{n-1,n} & b_{n-1,i+1} & \ldots & b_{n-1,n-1} \end{bmatrix} \tag{33}$$

In order for 31 to hold, in value, the ith column of D_i^* must be interchanged $n-i-1$ times to the nth column and multiplied by -1. This operation causes, $n-i$ sign changes in the value of the determinant. The sign of the cofactor $C_{n,i}$ is $(-1)^{n+i}$ so the signs and values are the same. Then

$$D_i^* = C_{n,i}. \tag{34}$$

Thus,

$$\frac{|B_{n\times n}|}{|B'_{n\times n}|} = \frac{b_n \cdot \vec{n}}{b'_n \cdot \vec{n}} \tag{35}$$

∇